# Modeling and Control of a Cyclo-Active-Bridge Inverter for Single-Stage Three-Phase Grid Interface

Tanuj Sen[◇], Mian Liao[◇], Yang Wu[†], and Minjie Chen[◇]
[◇]*Princeton University, Princeton, NJ, United States*
[†]*ABB Corporate Research, Västerås, Sweden, United States*
*Email: {tsen, minjie}@princeton.edu*

2025 IEEE Applied Power Electronics Conference and Exposition (APEC) | 979-8-3315-1611-6/25/$31.00 ©2025 IEEE | DOI: 10.1109/APEC48143.2025.10977218

***Abstract*—This paper presents the small-signal modeling and control of a cyclo-active-bridge (CAB) inverter for single-stage three-phase grid interface, featuring single-stage decoupled three-phase power flow control. The strengths of the CAB inverter and its control architecture include: (1) single-stage dc-ac power conversion; (2) highly integrated magnetic components; and (3) three independently controlled output phases. It allows for both balanced and unbalanced 3-Φ operation for grid forming and energy routing applications. The First Harmonic Approximation (FHA) method, along with the application of a correction factor, is used for finding an accurate small-signal model of the inverter. This small-signal model is then used to design a per-phase controller to control the per-phase output of the inverter as an ac output. A hardware prototype of this inverter is designed and tested in closed-loop to generate a 3-Φ ac output at 60 Hz.**

***Index Terms*—Cyclo-active-bridge inverter, three-phase, small-signal model, integrated magnetics, first harmonic approximation, correction factor, balanced operation, unbalanced operation**

## I. Introduction

With the rapid surge in energy demand as well as the growing need for switching to environmentally sustainable means of energy generation, the dependence on renewable sources of energy like solar or wind energy is ever increasing. These energy sources can be used to feed power directly into the existing grid infrastructure or can be used independently to meet the energy needs of small localized areas. Power electronic inverters are playing a critical role in interfacing these future energy systems either to the grid or for localized microgrid applications [1].

Conventional inverter designs usually involve single stage as well as multistage configurations with a low-pass filter at the output [2]–[4]. These inverters can be configured to operate either as a Grid-Forming Inverter (GFM), which directly control the grid voltage and frequency and provide a reference for the entire grid [5], or they can be used as Grid-Following Inverters (GFL), which primary feed power into the grid [6]. In this work, we present a 3-Φ cyclo-active-bridge (CAB) inverter which borrows on the concept of the dual active bridge (DAB) dc-dc converter. The primary side is composed of a three-phase dc-ac inverter with a cyclo-converter stage on the secondary side, connected by a three-phase transformer, as shown in Fig. 1. The topology is similar to the I3DAB dc-dc converter presented in [7]. The power flow can be controlled by changing the phase shift between the primary and secondary side voltages, similar to a DAB. This technique

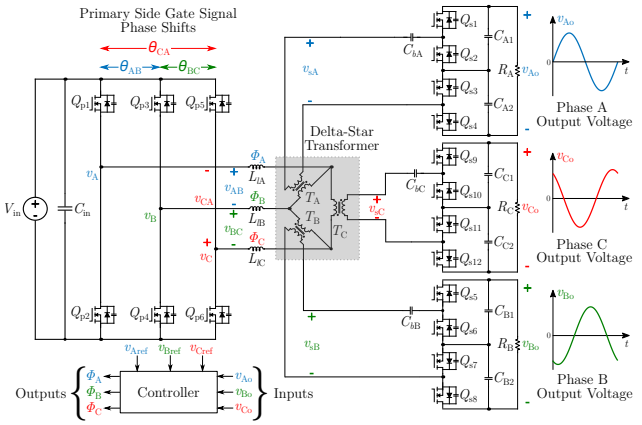


Fig. 1. Topology of the three-phase cyclo-active-bridge (CAB) inverter, with a four-switch cyclo-converter on each phase of the secondary side. Each phase generates a sinusoidal output voltage, while the power delivered by each phase can be controlled by the phase shift ($\phi_N$) between the primary side and secondary side voltages of the inverter. A dedicated controller is used to shape the sinusoidal voltage at the output of each phase. The transformer used is an integrated three-phase delta-star configuration transformer.

is used to shape the 60 Hz ac output, eliminating the need for a low-frequency output filter, and enabling more flexible 3-Φ power flow control. The advantage of this topology is that the three output ports are completely decoupled from each other in their operation, which allows for 1) single-stage power processing; 2) balanced and unbalanced 3-Φ operation, leading to a high control flexibility; 3) fast power response due to the high-frequency-link; and (4) direct phase-to-phase power flow without passing through the dc-port.

To control the operation of the CAB inverter as either a GFM or GFL inverter, a dedicated controller needs to be designed, which requires the extraction of the small-signal continuous-time model of the inverter. Previous research has extensively explored methods to derive the continuous-time model of the DAB converter [1], [8]–[10], which is useful for regulating the output voltage of the converter. [11], [12] use variations of the first harmonic approximation method to extract the small-signal converter model. In dc-dc applications, proportional-integral (PI) controllers are often used for controlling the converter output voltage. Proportional resonant (PR) controllers [13] find utility in dc-ac applications as they introduce infinite gain at the fundamental ac frequency. They

can also be used in combination with a PI controller, as in [14], to handle both dc and ac components at the output.

In this paper, the 3-Φ CAB inverter is introduced in detail in Section II. Due to its decoupled phase operation, it is treated as a single-phase dc-ac inverter and the First Harmonic Approximation (FHA) technique is employed for extracting its small-signal continuous-time model. The correction factor approach used in [12] is also employed to improve the accuracy of the extracted model, as shown in Section III. This model of the CAB inverter, at various output voltage levels, is then collectively used to design a suitable ac output voltage controller in Section IV, which is capable of generating a balanced or unbalanced 3-Φ ac output at the three decoupled output ports of the inverter. The operation of the designed closed-loop system is verified through both simulations and experimental results in Section V.

## II. Three Phase Cyclo-Active-Bridge Inverter: Overview

The Cyclo-Active-Bridge (CAB) inverter topology is shown in Fig. 1. This inverter takes a dc voltage as an input and converts it into three separate ac outputs, with galvanic isolation provided between the input and output by the three-phase transformer. The transformer also helps to provide a more flexible voltage conversion ratio between the input and the output. The operating principles and mechanism of the CAB inverter are closely derived from the operation of the half-bridge cyclo-converter based single phase dc-ac DAB inverter presented in [15], [16], and the 3-Φ dc-dc I3DAB converter topology introduced in [7]. Similar to as mentioned in [7] for the I3DAB topology, the primary side of the CAB inverter employs a three-phase half-bridge inverter, with the three phases connected in the delta configuration. The three phase switching signals of the primary side are equally phase shifted by 120° to generate a symmetrical three-level primary side voltage. The secondary side is composed of three separate phases, However, unlike [7], where each secondary side phase is composed of a full-bridge rectifier to generate a dc output voltage, the CAB inverter makes use of a cyclo-converter for each phase, similar to the implementation shown in [15]. This cyclo-converter allows for an ac output voltage at each of the three output phases. The frequency and amplitude of this ac ouptut voltage can be varied by properly controlling the value of the phase shift $\phi$ between the primary side and secondary side voltages. An advantage of the CAB inverter, derived from the I3DAB converter proposed in [7] due to their similar construction, is that the three output ports of such an inverter are isolated from each other and operate independently. This implies that the output voltage and power delivered by each phase can be independently controlled through the per-phase phase shift between the primary and secondary side transformer winding voltages, with no influence from the other two phases. Hence, the proposed 3-Φ inverter can be considered as three separated single phase dc-ac cyclo-inverters, with Fig. 2 highlighting the structure and the voltage and current waveforms of one of the three phases.

Due to the delta-configuration three-phase inverter on the primary side of the CAB inverter, with the per-phase switching

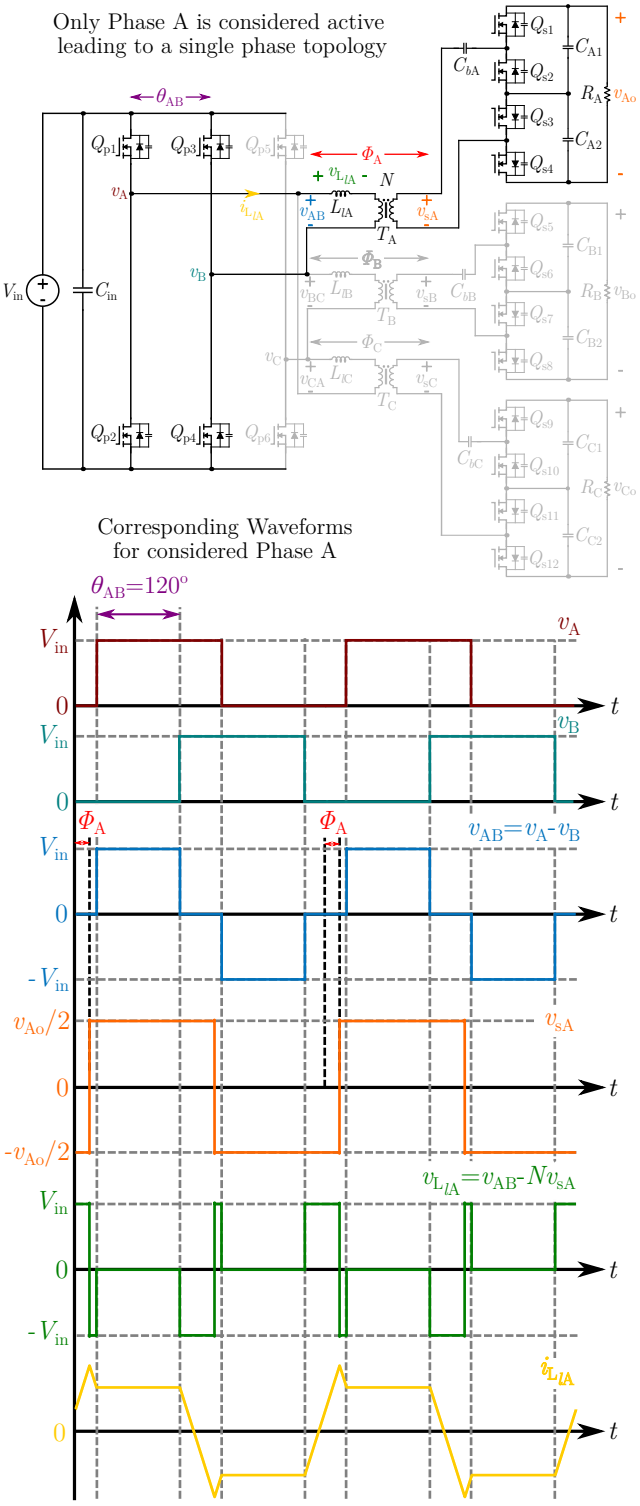


Fig. 2. The circuit diagram and the corresponding voltage and current waveforms in the linear mode of operation, with one of the output phases (Phase A) active. The primary side voltage $v_{AB}$ is a three-level voltage formed by the square-wave switch node voltages of phase A and B, which are phase-shifted by $\theta_{AB}$=120°. The secondary side voltage $v_{sA}$ is phase shifted ($\phi_A$) with respect to $v_{AB}$, which determines the voltage drop $L_{LlA}$ across the inductor $L_{lA}$, which in turn determines the current flowing through the inductor.

signals having a 120° phase shift between them, the per-phase primary side voltage is a symmetrical three-level voltage, formed by the phase shifted switch-node voltages of the two associated primary side half-bridge legs. On the other hand, the secondary side voltage of the CAB inverter is effectively a two-level square wave voltage with a peak amplitude of half of the output voltage. The phase shift per-phase phase shift $\phi$ between the primary and secondary side voltages is determined from the mid-point of the zero-level of the primary side voltage, as shown in Fig. 2. Due to the specific shapes of the primary and secondary side voltages, the per-phase operation of the CAB inverter can be divided into two separate modes or regimes, based on the value of the phase shift $\phi$ between the primary and secondary side voltage for each phase. These two modes are called the linear and non-linear mode of operation. In the linear mode of operation, which applies for the range $0 \leq |\phi| \leq \frac{\pi}{6}$, the per-phase power and the output voltage equations for the CAB inverter are as follows:

$$P_{\text{out}} = \frac{V_{\text{in}} V_{\text{out}}}{6\pi N L f_{\text{sw}}}\phi, \quad \forall \quad 0 \leq |\phi| \leq \frac{\pi}{6}. \tag{1}$$

$$V_{\text{out}} = \frac{V_{\text{in}} R_{\text{out}}}{6\pi N L f_{\text{sw}}}\phi. \tag{2}$$

where $V_{\text{in}}$ and $V_{\text{out}}$ are the input and output voltages, respectively. $L$ is the phase leakage inductance, $N$ refers to the transformer turns ratio, $f_{\text{sw}}$ is the switching frequency. Due to the linear relationship between the output power and the phase shift $\phi$, this regime of operation is called the linear mode. Note that this linear relationship exists only when the output voltage remains invariant. Furthermore, the linear relationship between the output voltage and $\phi$ is maintained only for constant load operation. On the other hand, for the range $\frac{\pi}{6} \leq |\phi| \leq \frac{\pi}{2}$, the per-phase power and output voltage with respect to $\phi$ are given as:

$$P_{\text{out}} = \frac{V_{\text{in}} V_{\text{out}}}{4\pi N L f_{\text{sw}}}(\phi - \frac{\phi^2}{\pi} - \frac{\pi}{36}), \quad \forall \quad \frac{\pi}{6} \leq |\phi| \leq \frac{\pi}{2}. \tag{3}$$

$$V_{\text{out}} = \frac{V_{\text{in}} R_{\text{out}}}{4\pi N L f_{\text{sw}}}(\phi - \frac{\phi^2}{\pi} - \frac{\pi}{36}). \tag{4}$$

which highlights the non-linear relationship between $P_{\text{out}}$, $V_{\text{out}}$ and $\phi$, hence the name non-linear mode for this regime of operation. The per-phase maximum power is attained at $\phi = \pi/2$, with the power curve being symmetrical around $\phi = \pi/2$, as shown in Fig. 3 (considering constant output voltage). Negative power flow can be achieved using negative values of $\phi$. Using these relations, the CAB inverter can be operated to produce an ac voltage at the output, by varying the phase shift $\phi$ accordingly. More details about the operation of the CAB inverter can be found in [17].

## III. Small Signal Modeling of the Three-Phase Cyclo-Active-Bridge Inverter

The extraction of the small-signal model of the CAB inverter is of great importance in order to design a suitable controller for controlling the output voltage to be ac. Since the three phases of the CAB inverter are completely decoupled from each other, the small-signal model can be developed on a per-phase basis, with each phase being treated as an equivalent single-phase DAB converter, as shown in Fig. 4. In this paper, we use the First Harmonic Approximation (FHA) technique to develop the small-signal model, along with the the use of the correction factor concept introduced in [12], to account for the higher order harmonics of the current and voltage which are neglected in the FHA. Moreover, due to the differing modes of operation of the CAB inverter with respect to $\phi$, the small-signal model needs to be developed separately for the linear mode and non-linear mode to correctly account for the varying system dynamics. We begin by considering the small-signal model for the linear mode and then extend the approach for the non-linear mode as well.

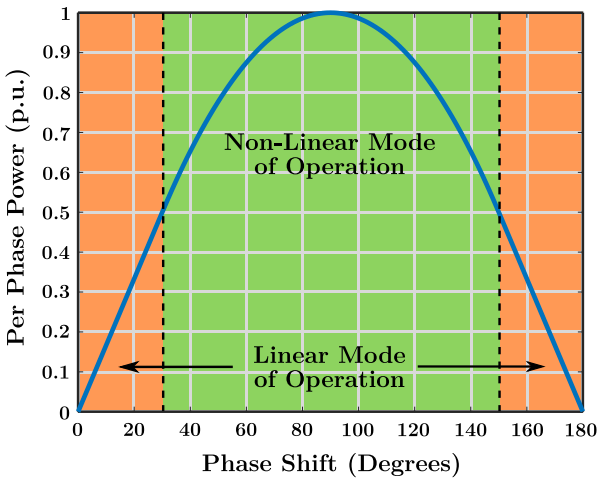


Fig. 3. Variation of the per-phase power (p.u.) with respect to the phase shift $\phi$ between the primary and secondary side voltages of the CAB inverter, assuming a constant output voltage.

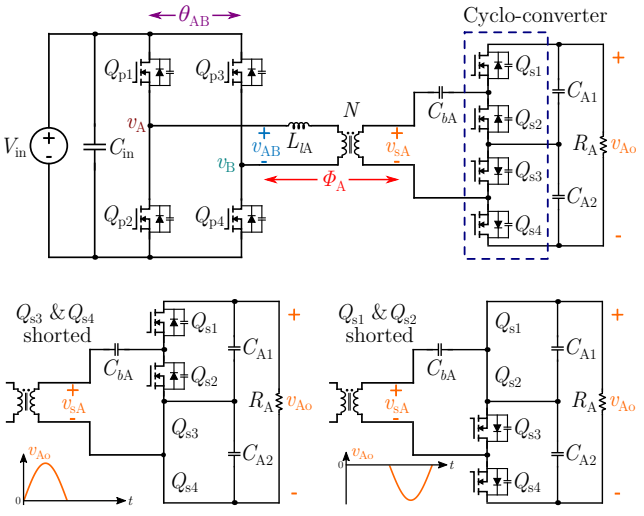


Fig. 4. A simplified single-phase model of the proposed 3-Φ CAB inverter, as the three phases are decoupled from each other. The operation principle of the cyclo-converter on the secondary side inverter is shown. The upper half-bridge operates conventionally while the lower half bridge is shorted when the output voltage is positive and vice-versa.

The per-phase primary and secondary side switched-mode voltages are shown in Fig. 2. The fundamental component, at the angular switching frequency of the inverter $\omega_s$, of the primary and secondary side voltages, $V_\mathrm{P}$ and $V_\mathrm{S}$, and the current through the inductor $i_\mathrm{L}$ are given as follows:

$$V_\mathrm{P} = \frac{4V_\mathrm{in}\sin\left(\frac{\pi}{3}\right)}{\pi}\sin\omega_s t. \tag{5}$$

$$V_\mathrm{S} = \frac{4v_\mathrm{o}}{2\pi N}\sin(\omega_s t-\phi) = v_\mathrm{s}\sin\omega_s t + v_\mathrm{c}\cos\omega_s t. \tag{6}$$

$$\frac{di_\mathrm{L}}{dt} = \frac{V_\mathrm{P}-V_\mathrm{S}}{L}. \tag{7}$$

Note that $V_S$ has a factor of the turns ratio of the transformer $N$ as it is referred to the primary side of the inverter. From (5) and (6), it is evident that the fundamental components of the primary and secondary side voltages are also phase shifted by $\phi$. As a result, $V_\mathrm{S}$ has a sine ($v_\mathrm{s}$) and a cosine ($v_\mathrm{c}$) component, which also leads to the inductor current $i_\mathrm{L}$ to be composed of a sine ($i_\mathrm{Ls}$) and a cosine ($i_\mathrm{Lc}$) component. Thus, the fundamental component of the inductor current and its differential become:

$$i_\mathrm{L} = i_\mathrm{Lc}\cos\omega_s t + i_\mathrm{Ls}\sin\omega_s t. \tag{8}$$

$$\frac{di_\mathrm{L}}{dt} = \left(\frac{di_\mathrm{Lc}}{dt}+\omega_s i_\mathrm{Ls}\right)\cos\omega_s t + \left(\frac{di_\mathrm{Ls}}{dt}-\omega_s i_\mathrm{Lc}\right)\sin\omega_s t. \tag{9}$$

The current flowing into the inverter output capacitor can be computed as the product of the inductor current referred to the secondary side and the switching signal of the cyclo-converter. Since the switching signal is practically a square wave with a duty ratio of 50%, phase shifted by $\phi$, its fundamental component representation is:

$$s_2 = \frac{1}{2} - \frac{2}{\pi}\sin\phi\cos\omega_s t + \frac{2}{\pi}\cos\phi\sin\omega_s t. \tag{10}$$

When multiplied with the secondary side current, we get:

$$s_2\cdot\frac{i_\mathrm{L}}{N} = -\frac{i_\mathrm{Lc}}{N\pi}\sin\phi + \frac{i_\mathrm{Ls}}{N\pi}\cos\phi + \text{harmonic terms}. \tag{11}$$

Since the output capacitor voltage is practically dc, we consider only the zeroth-order components of currents and the voltages, leading to the following governing equation for the output voltage:

$$C_\mathrm{O}\frac{dv_\mathrm{o}}{dt} = -\frac{i_\mathrm{Lc}}{N\pi}\sin\phi + \frac{i_\mathrm{Ls}}{N\pi}\cos\phi + \frac{v_\mathrm{o}}{R_\mathrm{out}}. \tag{12}$$

Considering $i_\mathrm{Ls}$, $i_\mathrm{Lc}$ and $v_\mathrm{o}$ to be the state variables of the system, we arrive at the following state equations:

$$\frac{di_\mathrm{Ls}}{dt} = \frac{4V_\mathrm{in}}{\pi L}\sin\frac{\pi}{3} - \frac{4v_\mathrm{o}}{2\pi NL}\cos\phi + \omega_s i_\mathrm{Lc} \tag{13}$$

$$\frac{di_\mathrm{Lc}}{dt} = \frac{4v_\mathrm{o}}{2\pi NL}\sin\phi - \omega_s i_\mathrm{Ls} \tag{14}$$

$$\frac{dv_\mathrm{o}}{dt} = -\frac{i_\mathrm{Lc}}{C_\mathrm{O}N\pi}\sin\phi + \frac{i_\mathrm{Ls}}{C_\mathrm{O}N\pi}\cos\phi + \frac{v_\mathrm{o}}{R_\mathrm{out}C_\mathrm{O}}. \tag{15}$$

These equations only take the fundamental components of the voltages and the current into account. However, by neglecting the effect of the higher order harmonics, the small-signal model would lack the desired accuracy and would fail to model the variation of the system transfer function with a changing output voltage. Therefore, we make use of a correction factor $\gamma$ for the state variables, introduced in [12], to account for the effect of these additional harmonics. The power transfer between the primary and secondary side, considering the two fundamental frequency sources $V_\mathrm{P}$ and $V_\mathrm{S}$, connected by the inductance $L$ is given as:

$$P_{\text{out}(1)} = \frac{4V_\mathrm{in}v_\mathrm{o}}{\pi^2\omega_s NL}\sin\left(\frac{\pi}{3}\right)\sin\phi. \tag{16}$$

while the actual power flow in the linear-mode is given by (1). Therefore, dividing (1) by (16), we get the required correction factor $\gamma$ for $v_o$:

$$\gamma = \frac{P_\mathrm{out}}{P_{\text{out}(1)}} = \frac{\pi^2\phi}{12\sin\left(\frac{\pi}{3}\right)\sin\phi}. \tag{17}$$

$$v_{\text{o,mod}} = \gamma v_\mathrm{o}. \tag{18}$$

In a similar manner, the correction factor for $i_\mathrm{Ls}$, $i_\mathrm{Lc}$ can be determined. The total active power delivered by the fundamental component of the inductor current depends solely on $i_\mathrm{Ls}$ and is given as:

$$P_{\text{out}(1)} = \frac{1}{2}\frac{4V_\mathrm{in}i_\mathrm{Ls}}{\pi\omega_s L}\sin\left(\frac{\pi}{3}\right)\sin\phi. \tag{19}$$

Based on (19), we find the correction factor for $i_\mathrm{Ls}$ to be $\gamma$ as well, leading to the following corrected state variable relation:

$$i_{\text{Ls,mod}} = \gamma i_\mathrm{Ls}. \tag{20}$$

Lastly, the corrected form of $i_\mathrm{Lc}$ is calculated by comparing the values of the total reactive power to the reactive power due to the fundamental component of the current, in a manner similar to that shown in [12], leading to the following relation:

$$i_{\text{Lc,mod}} = \gamma i_\mathrm{Lc} + (\gamma-1)\frac{4V_\mathrm{in}}{\pi\omega_s L}. \tag{21}$$

Using the aforementioned relations, the modified state equations can be formulated, as shown below:

$$\frac{di_{\text{Ls,mod}}}{dt} = \frac{4V_\mathrm{in}}{\pi L}\sin\frac{\pi}{3} - \frac{4V_{\text{out,mod}}}{2\pi NL}\cos\phi + \omega_s i_{\text{Lc,mod}}. \tag{22}$$

$$\frac{di_{\text{Lc,mod}}}{dt} = \frac{4v_{\text{o,mod}}}{2\pi NL}\sin\phi - \omega_s i_{\text{Ls,mod}} + \frac{d\frac{4(\gamma-1)V_\mathrm{in}}{\omega_s\pi L}\sin\left(\frac{\pi}{3}\right)}{dt}. \tag{23}$$

$$\frac{dv_{\text{o,mod}}}{dt} = -\frac{i_{\text{Lc,mod}}}{C_\mathrm{O}N\pi}\sin\phi + \frac{i_{\text{Ls,mod}}}{C_\mathrm{O}N\pi}\cos\phi + \frac{v_{\text{o,mod}}}{R_\mathrm{out}C_\mathrm{O}} + \frac{4(\gamma-1)V_\mathrm{in}}{\omega_s\pi^2 LC_\mathrm{O}}\sin\left(\frac{\pi}{3}\right)\sin\phi. \tag{24}$$

Upon perturbing the state-space variables and $\phi$ in the modified state-space equations, we arrive at the following state-space matrices for the small signal model.

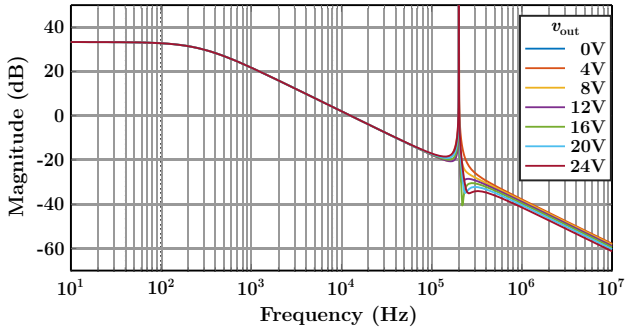


Fig. 5. Magnitude response of the per-phase small-signal transfer function $G_{v_o\phi}(s)$ of the CAB inverter for different output voltages, in the linear mode.

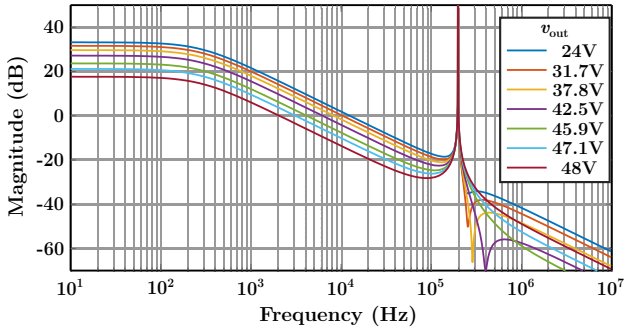


Fig. 6. Magnitude response of the per-phase small-signal transfer function $G_{v_o\phi}(s)$ of the CAB inverter for different output voltages, in the non-linear mode. The gain of the system varies with the output voltage.

$$A = \begin{bmatrix} 0 & \omega_s & \frac{-4\cos\phi}{2\pi NL} \\ -\omega_s & 0 & \frac{4\sin\phi}{2\pi NL} \\ \frac{\cos\phi}{N\pi C_O} & \frac{-\sin\phi}{N\pi C_O} & \frac{-1}{R_{out}C_O} \end{bmatrix} \tag{25}$$

$$B = \begin{bmatrix} \frac{-4V_{out}\sin\phi}{2\pi NL} \\ \frac{-4V_{out}\cos\phi}{2\pi NL} + \frac{4V_{in}}{\omega_s\pi L}\sin\left(\frac{\pi}{3}\right)\lambda\frac{d}{dt} \\ -\frac{i_{Lc}}{C_O N\pi}\cos\phi - \frac{i_{Ls}}{C_O N\pi}\sin\phi + \frac{4V_{in}\lambda}{\omega_s\pi^2 NLC_O}\sin\left(\frac{\pi}{3}\right)\sin\phi \end{bmatrix} \tag{26}$$

$$C = \begin{bmatrix} 0 & 0 & 1 \end{bmatrix} \tag{27}$$

for the state-space matrix $x = [i_{\text{Ls,mod}}\ i_{\text{Lc,mod}}\ v_{\text{o,mod}}]^T$ and the input matrix $x = [\phi]$. The parameter $\lambda$ in $B$ is defined as:

$$\lambda = \frac{\pi^2}{12\sin\frac{\pi}{3}\sin\phi} - \frac{\cos\phi}{\sin\phi}. \tag{28}$$

Therefore, the small-signal transfer function relating the output voltage $v_o$ to the phase shift $\phi$ for the linear mode of operation for the CAB inverter can be computed through:

$$G_{v_o\phi}(s) = C(s\cdot I - A)^{-1}B. \tag{29}$$

The bode plot showing the magnitude response of the each phase of the CAB inverter system, when operating in the linear mode, is computed and shown in Fig. 5. For the magnitude response, the following per-phase inverter parameters were selected: a switching frequency $f_{sw}$ of 200 kHz to generate a 48 V ac voltage at the output terminals of each phase, with a phase inductance $L$ of 5 $\mu$H, a transformer turns ratio $N$ of 1.33, an input voltage of 48 V, while $C_{load}$ and $R_{load}$ are 24 $\mu$F and 23 $\Omega$, respectively. The per-phase magnitude response is shown for varying output voltage values, as is the case for ac operation. However, the voltage variation is only taken from 0 V to 24 V, as this is the range of linear-mode of operation. From the magnitude response, it is evident that the gain of the system at lower frequencies remains constant with respect to the output voltage, which is a characteristic of the linear-mode of operation. Since the considered system is undamped, a large resonance peak appears at the switching frequency.

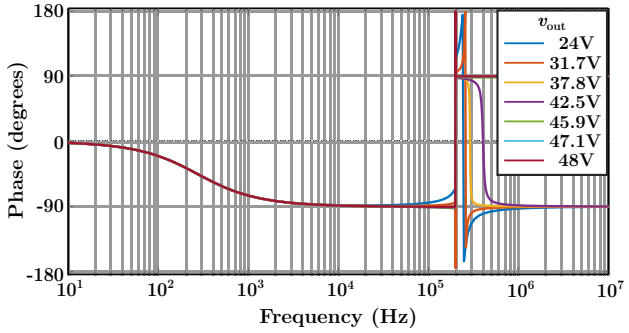


Fig. 7. Phase response of the per-phase small-signal transfer function $G_{v_o\phi}(s)$ of the CAB inverter for different output voltages, in the non-linear mode of operation. The phase of the system shows a spike at the switching frequency.

In a similar manner, the per-phase system transfer function for the CAB inverter can be derived for the non-linear mode of operation. All the state equations have the same form as the linear-mode. However, due to the per-phase power equation being different for the non-linear mode (3), the value of the correction factor is different for this mode:

$$\gamma = \frac{P_{out}}{P_{out(1)}} = \frac{\pi^2(\phi - \frac{\phi^2}{\pi} - \frac{\pi}{36})}{8\sin\left(\frac{\pi}{3}\right)\sin\phi}. \tag{30}$$

The resulting state-space matrices for the non-linear mode have the same form as the linear-mode matrices as given in (25), (26) and (27). However, the value of $\lambda$ in this small-signal model is different, due to the different value of the correction factor $\gamma$ in this mode of operation. The non-linear mode value of $\lambda$ is given as:

$$\lambda = \frac{\pi(\pi - 2\phi)}{8\sin\frac{\pi}{3}\sin\phi} - \frac{\cos\phi}{\sin\phi}. \tag{31}$$

Using this value of $\lambda$ in the state-space matrices and then applying these matrices to (29), the per-phase transfer function $G_{v_o\phi}(s)$ for the non-linear mode of operation can be determined. The bode magnitude plot for $G_{v_o\phi}(s)$ for varying output voltages $v_o$ in the non-linear range is shown in Fig. 6. In

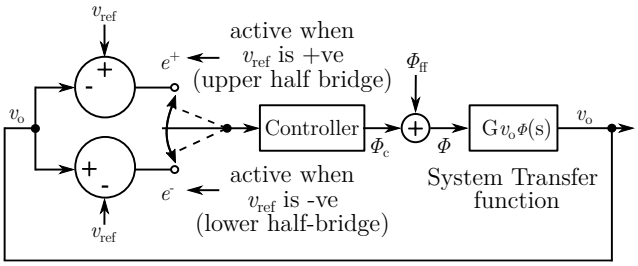


Fig. 8. Block diagram of the per phase closed loop system with the controller. The polarity of the processed error signal depends on the polarity of the reference signal, which also influences which half of the cyclo-converter is active. The controller takes this error as an input and converts it into the required phase shift between the primary and secondary side voltages.

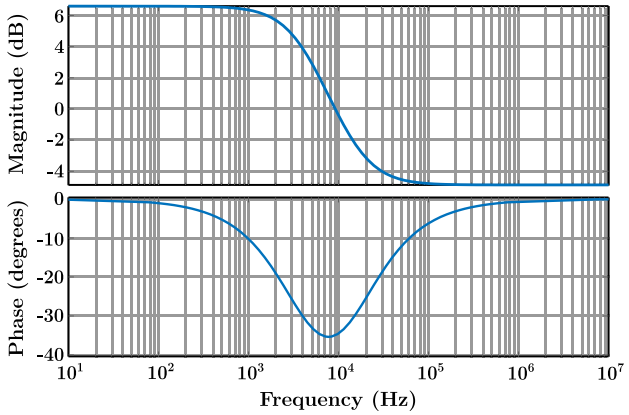


Fig. 9. Magnitude and phase response of the designed per-phase controller $G_{ovc}(s)$ for the CAB inverter. The lag compensator introduces a phase dip around the desired crossover frequency of $f_{sw}/20 = 10$ kHz, which allows the system to have a phase margin of around 60° for all output voltages.

the non-linear mode of operation, the gain of the system varies with the output voltage. This is due to $\lambda$ having a factor of the phase-shift $\phi$ in it, and the value of $\lambda$ has a direct correlation with the gain of the system. Hence, as $\phi$ is varied to change the output voltage, the gain of the system changes.

The phase variation of the system over frequency of operation, for output voltages in the non-linear mode of operation, is shown in Fig. 7. The phase variation is independent of any changes in the output voltage and only shows a jump at the switching frequency. The phase variation shows the same characteristic for the linear mode of operation as well. The phase information is of great importance for designing a suitable closed-loop controller for the CAB inverter, as is shown in the following section.

## IV. Controller Design for the CAB Inverter

Figure 4 shows the operation of the cyclo-converter on the secondary side (per-phase) of the CAB inverter to generate an ac voltage at the output, by varying the phase shift $\phi$ accordingly. To generate both positive and negative voltages at the output, the voltage reference needs to be positive for one half of the desired ac voltage period and negative for the other half. Thus, the error signal that is fed into the controller needs to have the proper polarity, as is shown in Fig. 8. Since the frequency of the output ac voltage is many orders of magnitude lower than the switching frequency, the CAB inverter can effectively be treated as a dc-dc converter. Therefore, the magnitude and phase responses shown in the previous section can be used collectively to design a per-phase controller, which can modulate the output voltage of the phase as an ac voltage of required amplitude and frequency.

Due to the variable gain of the system in the non-linear mode, the crossover frequency will be different for different output voltages. In this case, we choose the system magnitude response with the highest gain ($v_{out}$ = 24 V) as the basis in order to compute the required gain of the controller, so that the crossover frequency of the modulated system shifts to $f_{sw}/20$. This would cause the crossover frequency of the modulated system to be lower than $f_{sw}/20$ at other output voltages, which effectively attenuates the impact of switching frequency disturbances on the closed loop system.

An important aspect for controller design is to ensure suitable gain and phase margin for the system. To design the controller, a phase margin of 60° is chosen at the desired crossover frequency. A lag compensator is designed to this effect. The pole and zero of the lag compensator are chosen such that the phase margin of the system at different output voltages remains in the vicinity of the 60° target. The designed per-phase controller, therefore, has the following form, with the mentioned values:

$$G_{\text{ovc}}(s) = K_{\text{p}}\left(\frac{s+\omega_{\text{z}}}{s+\omega_{\text{p}}}\right) = \frac{1}{1.754}\left(\frac{s+2\pi\cdot 15\ kHz}{s+2\pi\cdot 4\ kHz}\right) \quad (32)$$

The magnitude and phase response of the designed controller are shown in Fig. 9. The designed controller responds to any small signal variations in the output voltage. The phase shift value generated by the controller, together with a feedforward value of the phase shift, which accounts for the large signal variation of the output voltage when operating to produce an ac output, regulates the output voltage of each phase, as shown in Fig. 8.

## V. Simulations and Experimental Verification

The operation of the 3-Φ cyclo-active-bridge circuit, as shown in Fig. 1, was simulated in PLECS, with the circuit parameter values mentioned previously in Section III. The switching frequency for the inverter was selected as 200 kHz, similar to the value taken in the small-signal model design. In order to get an ac output at the three phases of the CAB inverter, the designed per-phase controller was employed, operating each phase in a closed loop, independent of the other phases. This closed-loop controlled inverter is first simulated to generate a 3-Φ 48 V balanced ac output at 60 Hz for an input voltage of 48 V dc. The simulation results for the balanced case are provided in Fig. 10. The simulation results show that the designed per-phase controller is able to shape the output voltage of each phase of the inverter into the desired sinusoidal voltage with an amplitude of 48 V and a phase shift of 120° between each of the three phases, resulting in a balanced 3-Φ output. To highlight the capability of the designed closed-l oop

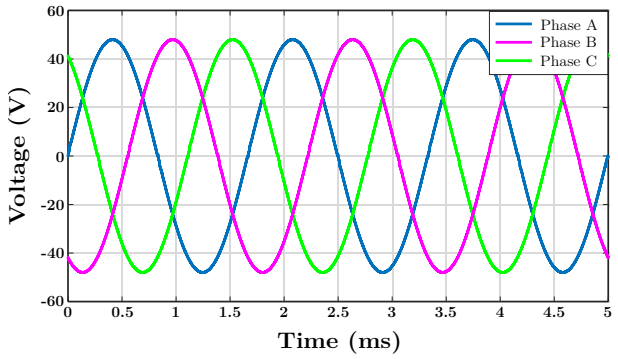


Fig. 10. Simulation results showing the desired operation of the 3-Φ output voltages of the inverter in the closed loop. The designed per phase controller creates a per phase sinusoidal voltage with an amplitude of 48 V at 60 Hz, with a phase shift of 120° between them.

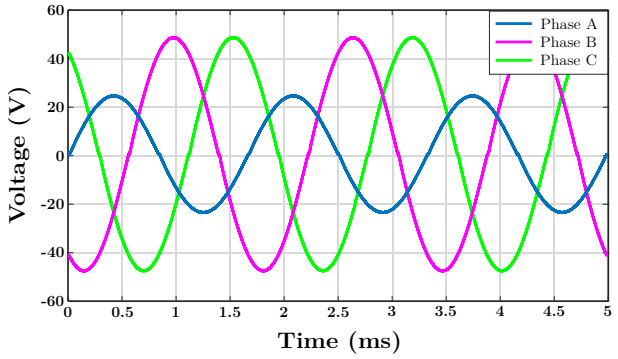


Fig. 11. Simulation results showing the unbalanced closed loop operation of the 3-Φ inverter. The controller for Phase A holds its output voltage at 24 V 60 Hz, while Phase B and Phase C output voltages are at 48 V and 60 Hz. The phase shift between the phases is maintained at 120°.

inverter to operate with an unbalanced 3-Φ output, the inverter is driven with three sinusoidal voltage references which are 120° shifted with respect to each other. However, the reference for Phase A is set to have an amplitude of 24 V, while Phase B and Phase C reference amplitudes are set as 48 V. The unbalanced operation simulation results, with Phase A voltage having half the amplitude of Phase B and Phase C voltages, in accordance with the provided references, are shown in Fig. 11.

The designed inverter circuit was also implemented on hardware, with the experimental prototype shown in Fig. 12. Each switch on the primary side of the inverter was realized with two 100 V/90 A GS61008P GaN MOSFETs in parallel, while the switches on the secondary side make use of the 650 V/30 A GS66508B GaN MOSFETs provided by GaN systems. The phase inductance of 5 $\mu$H was designed with a 3F46 planar ER core with litz wire windings, while the transformer makes use of a 3C92 planar ER core with PCB windings for the primary side and litz wire for the secondary side windings. The TMS320F28379D control card provided by Texas Instruments is used for generating the gate signals and for implementing the closed loop control. The three output phases of the inverter are connected to three separate resistive loads. The full dc-rated 300 W 3-Φ experimental setup is

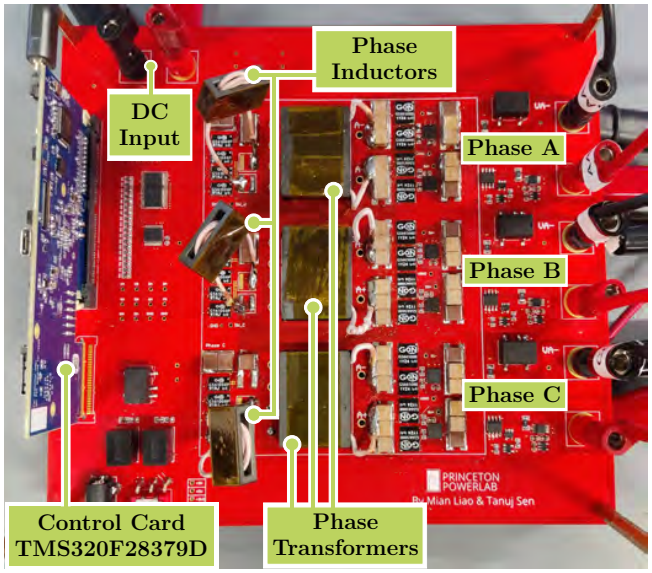


Fig. 12. Hardware prototype of the cyclo-converter based 3-Φ CAB inverter. The primary side terminals of the transformers are routed on the PCB and are connected in a delta configuration, while the secondary side terminals are formed using litz wires, connected separately to three independent secondary side phases without balancing needs.

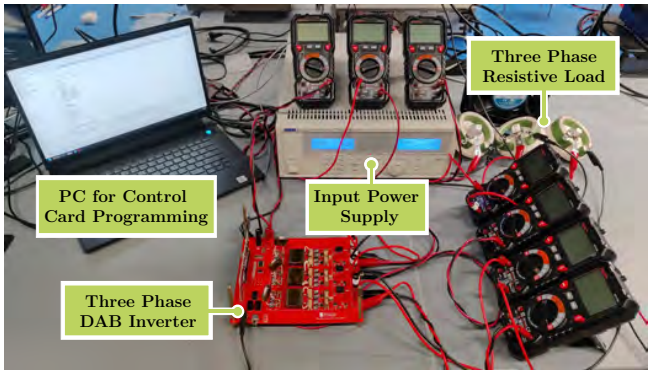


Fig. 13. Complete hardware setup of the cyclo-converter based 3-Φ CAB inverter, with the three output phases of the inverter connected three equal resistive loads of 50 Ω each, simulating a balanced load at the output. The inverter is provided a dc supply of 48 V at the input. The control card TMS320F28379D implements the closed loop control to produce a 3-Φ ac voltage at the output.

shown in Fig. 13.

Similar to the simulation results, the experimental results for the inverter being controlled to provide a balanced 3-Φ output voltage at 48 V and 60 Hz are shown in Fig. 14. At every zero crossing of the per phase output voltage, there is a slight discontinuity which appears due to change in the active half-bridge of the cyclo-converter on the secondary side, as depicted in Fig. 4 previously. Additionally, the unbalanced operation of the inverter was also tested through experiments, the results of which are provided in Fig. 15. In this case, Phase A is completely turned off, while Phase B and Phase C are controlled to produce a sinusoidal output voltage with an amplitude of 48 V at 60 Hz. Even in this case, the discontinuity at the zero crossing of the phase voltages, due to the bridge

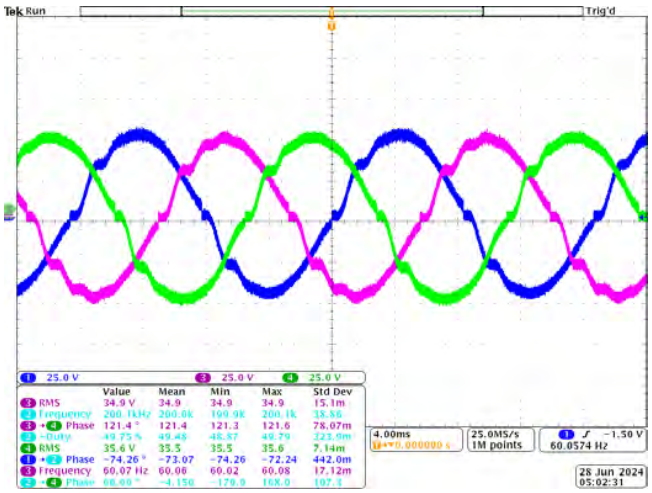


Fig. 14. Experimental results showing the 3-Φ output voltages of the inverter, with the per phase controller set to create a per phase 60 Hz sinusoidal voltage with an amplitude of 48 V. The three phases are shifted of 120° among each other.

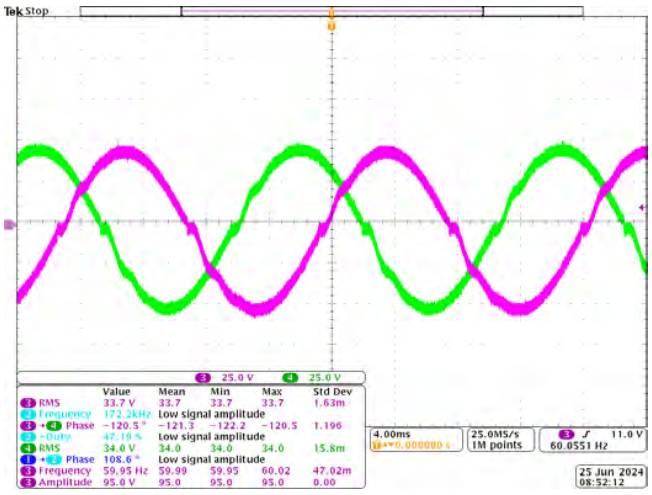


Fig. 15. Experimental results showing the unbalanced 3-Φ output voltages of the inverter, with the per phase controllers for Phase B and Phase C set to create a per phase 60 Hz sinusoidal voltage with an amplitude of 48 V, while Phase A is completely turned off. The phase shift between Phase B and Phase C output voltages is still maintained at 120°.

switching action of the cyclo-converter, is observable. The experimental results verify the versatility of the designed inverter in producing both balanced and unbalanced 3-Φ ac output voltages.

## VI. Conclusion

The small-signal modeling using the First Harmonic Approximation technique and control design of the single-stage 3-Φ cyclo-active-bridge inverter is presented in this paper. The three phases of the inverter are isolated from each other, thus, this inverter can be used for both balanced and unbalanced 3-Φ operation. Moreover, due to this decoupled nature, a dedicated per phase controller can be designed for each of the three phases, allowing each phase to be controlled similar to a 1-Φ inverter. A prototype of the CAB inverter is designed on hardware, using integrated magnetics and its operation is tested at a frequency of 200 kHz. Simulations as well as experimental measurements show that the closed loop operation of the proposed inverter topology, using the per-phase controller designed for the CAB inverter is indeed capable of generating both balanced and unbalanced 3-Φ ac output voltages at 60 Hz.

## Acknowledgements

This work was supported by NSF ASCENT Grant Award Number #2328241 and the NJEDA Wind Institute Fellowship.

## References

[1] J. Yang, S. Guenter, G. Buticchi, C. Gu, M. Liserre, and P. Wheeler, "On the impedance and stability analysis of dual-active-bridge-based input-series output-parallel converters in dc systems," *IEEE Transactions on Power Electronics*, vol. 38, no. 8, pp. 10 344–10 358, 2023.

[2] S. Anttila, J. S. Döhler, J. G. Oliveira, and C. Boström, "Grid forming inverters: A review of the state of the art of key elements for microgrid operation," *Energies*, vol. 15, no. 15, 2022. [Online]. Available: https://www.mdpi.com/1996-1073/15/15/5517

[3] P. Morsali, S. Dey, A. Mallik, and A. Akturk, "Switching modulation optimization for efficiency maximization in a single-stage series resonant dab-based dc–ac converter," *IEEE Journal of Emerging and Selected Topics in Power Electronics*, vol. 11, no. 5, pp. 5454–5469, 2023.

[4] S. Jain and V. Agarwal, "A single-stage grid connected inverter topology for solar pv systems with maximum power point tracking," *IEEE Transactions on Power Electronics*, vol. 22, no. 5, pp. 1928–1940, 2007.

[5] L. Kong, Y. Xue, L. Qiao, and F. Wang, "Control design of passive grid-forming inverters in port-hamiltonian framework," *IEEE Transactions on Power Electronics*, vol. 39, no. 1, pp. 332–345, 2024.

[6] D. Pattabiraman, R. H. Lasseter., and T. M. Jahns, "Comparison of grid following and grid forming control for a high inverter penetration power system," in *2018 IEEE Power Energy Society General Meeting (PESGM)*, 2018, pp. 1–5.

[7] J. Böhler, F. Krismer, T. Sen, and J. W. Kolar, "Optimized modulation of a four-port isolated dc–dc converter formed by integration of three dual active bridge converter stages," in *2018 IEEE International Telecommunications Energy Conference (INTELEC)*, 2018, pp. 1–8.

[8] S. S. Shah and S. Bhattacharya, "A simple unified model for generic operation of dual active bridge converter," *IEEE Transactions on Industrial Electronics*, vol. 66, no. 5, pp. 3486–3495, 2019.

[9] O. M. Hebala, A. A. Aboushady, K. H. Ahmed, S. Burgess, and R. Prabhu, "Generalized small-signal modelling of dual active bridge dc/dc converter," in *2018 7th International Conference on Renewable Energy Research and Applications (ICRERA)*, 2018, pp. 914–919.

[10] M. Safayatullah and I. Batarseh, "Small signal model of dual active bridge converter for multi-phase shift modulation," in *2020 IEEE Energy Conversion Congress and Exposition (ECCE)*, 2020, pp. 5960–5965.

[11] H. Qin and J. W. Kimball, "Generalized average modeling of dual active bridge dc–dc converter," *IEEE Transactions on Power Electronics*, vol. 27, no. 4, pp. 2078–2084, 2012.

[12] S. S. Shah and S. Bhattacharya, "Large small signal modeling of dual active bridge converter using improved first harmonic approximation," in *2017 IEEE Applied Power Electronics Conference and Exposition (APEC)*, 2017, pp. 1175–1182.

[13] H. Cha, T.-K. Vu, and J.-E. Kim, "Design and control of proportional-resonant controller based photovoltaic power conditioning system," in *2009 IEEE Energy Conversion Congress and Exposition*, 2009, pp. 2198–2205.

[14] H. Qin and J. W. Kimball, "Closed-loop control of dc–dc dual-active-bridge converters driving single-phase inverters," *IEEE Transactions on Power Electronics*, vol. 29, no. 2, pp. 1006–1017, 2014.

[15] A. Trubitsyn, B. J. Pierquet, A. K. Hayman, G. E. Gamache, C. R. Sullivan, and D. J. Perreault, "High-efficiency inverter for photovoltaic applications," in *2010 IEEE Energy Conversion Congress and Exposition*, 2010, pp. 2803–2810.

[16] B. J. Pierquet and D. J. Perreault, "A single-phase photovoltaic inverter topology with a series-connected energy buffer," *IEEE Transactions on Power Electronics*, vol. 28, no. 10, pp. 4603–4611, 2013.

[17] M. Liao, T. Sen, Y. Wu, and M. Chen, "Analysis and design of a cyclo-active-bridge inverter for single-stage three-phase grid interface," in *2025 IEEE Applied Power Electronics Conference and Exposition (APEC)*, 2025.